

PACS numbers: 78.67.Bf; 79.20.Eb; 87.16.dp; 87.80.Dj
DOI: 10.1070/QE2012v042n05ABEH014853

Photothermal effects induced by laser heating of gold nanorods in suspensions and inoculated tumours during *in vivo* experiments

G.S. Terentyuk, A.V. Ivanov, N.I. Polyanskaya, I.L. Maksimova, A.A. Skaptsov, D.S. Chumakov, B.N. Khlebtsov, N.G. Khlebtsov

Abstract. **Photothermal effects are studied under laser irradiation of aqueous suspensions of gold nanorods (*in vitro* experiments) and mice-inoculated Erlich carcinoma after intravenous injection of gold nanorods with the size 40 × 10 nm and plasmon resonance at the wavelength 810 nm (in vivo experiment). In 24 hours after the injection the polyethylene-glycol-coated nanoparticles accumulated in the tumour with the concentration three – four times greater than in healthy muscle tissue. At concentrations, attained as a result of passive accumulation of nanoparticles in the tumour (4 μg per 1 g of tumour), the efficiency of the tumour heating was higher than that in aqueous solutions having the same concentration of nanoparticles. Various mechanisms of this effect are discussed including the difference in thermal physical parameters of water and biotissue, the aggregation of nanoparticles in tissues, the influence of multiple scattering in biotissue, and the nonuniform accumulation of particles in the tumour. Using the Monte Carlo method for simulating multiple scattering of light, it is shown that there are such proportions between the biotissue scattering coefficient and the absorption coefficient of nanoparticles, at which the fraction of absorbed photons in the tissue is higher than that in a transparent medium containing the same nanoparticles. The conclusion is made that the regime of hyperthermia is less efficient for antineoplastic therapy than the thermal damage due to fast short-time heating of the tissues up to the destruction temperature.**

Keywords: *gold nanoparticles, photothermal effect, photothermal therapy of tumour.*

G.S. Terentyuk N.G. Chernyshevsky Saratov State University (National Research University), ul. Astrakhanskaya 83, 410012 Saratov, Russia; Ulyanovsk State University, ul. Tolstogo 42, 432970 Ulyanovsk, Russia;
A.V. Ivanov, N.I. Polyanskaya N.N. Blokhin Russian Cancer Research Centre, Russian Academy of Medical Sciences, Kashirskoe sh. 24, 115478 Moscow, Russia;
I.L. Maksimova, A.A.Skaptsov, D.S. Chumakov N.G. Chernyshevsky Saratov State University (National Research University), ul. Astrakhanskaya 83, 410012 Saratov, Russia;
B.N. Khlebtsov Institute of Biochemistry and Physiology of Plants and Microorganisms, Russian Academy of Sciences (IBPPM RAS), prosp. Entuziastov 13, 410049 Saratov, Russia;
N.G. Khlebtsov N.G. Chernyshevsky Saratov State University (National Research University), 83, ul. Astrakhanskaya 83, 410012 Saratov, Russia; Institute of Biochemistry and Physiology of Plants and Microorganisms, Russian Academy of Sciences (IBPPM RAS), prosp. Entuziastov 13, 410049 Saratov, Russia;
e-mail: khlebtsov@ibppm. sgu.ru

Received 23 March 2012
Kvantovaya Elektronika **42** (5) 380–389 (2012)
Translated by V.L. Derbov

1. Introduction

Depending on the mechanism of damaging the pathological biotargets (organs, tissues, cells) the method of thermotherapy [1] was used in two versions: hyperthermia and thermodestruction (thermolysis). In hyperthermia the heating of biotargets up to the temperature of 43–45 °C is used, which can lead to the cell apoptosis due to breaking the normal cell functions, the denaturation of enzymes, the induction of thermal shock proteins, the blood circulation disturbance, the reduction of the rate of damage reparation in malignant cells compared to normal tissues, etc. [1]. In the case of the thermolysis (thermodestruction) the heating up to more than 50 °C is implemented in a definite area of a tissue or organ, affected by a pathological process. This thermal impact, as a rule, is local and short-time. The use of thermolysis is most urgent in oncology, where it leads to necrosis of malignant cells and tumour destruction [2].

The variety of methods, using which the thermotherapy is implemented, is associated with the variety of radiation sources and thermal-sensitising agents that absorb radiation and release heat, used for hyperthermia or thermolysis [1]. One of the relatively new and promising methods for implementing the tissue thermolysis is the plasmon-resonance photothermotherapy (PPTT) [3, 4], based on the laser heating of metal, mostly gold and composite (dielectric-gold, silver-gold), nanoparticles. As shown in pioneering work [5], the local heating of colloid gold particles with the size ~20 nm, adsorbed at the surface of malignant cells, causes their death after exposure to green pulsed laser radiation with a relatively low mean power, but high enough peak power of short (20 ns) pulses. A similar result was obtained [6] for cancer cells, labelled with gold nanoshells and exposed to red laser light in the cw regime. The high efficiency of heating is determined by the large absorption cross section of metal nanoparticles at the plasmon resonance wavelength [7], which is by many orders of magnitude higher than that of endogenous thermal-sensitising chromophores of the melanin type.

To date the methods are developed providing the chemical synthesis of particles with the plasmon resonance that can be tuned into a required spectral range, including the biotissue transparency window (650–900 nm) [8, 9], by varying the composition and the structure of the particles. From the entire variety of nanoparticles used now for PPTT one may select three classes of most promising particles, namely, gold nanoshells on silicon dioxide cores [10], gold–silver nanocages [11], and gold nanorods [12, 13]. Gold nanoshells are the most investigated nanoparticles from the point of view of their application in PPTT; the information about them may

be found in recent reviews [14, 15], including the published data of *in vitro* and *in vivo* experiments [16–18]. That is why exactly these particles were chosen by Nanospectra Biosciences (USA) to begin the first clinical testing of PPTT in application to malignant tumours of head and neck of a human [19].

In 2007 the team of Y.Xia [20] first demonstrated the use of gold–silver nanocages for PPTT of cancer cells *in vivo* (the data on optoacoustical imaging of melanoma in the in vivo experiment were published in [21], and a detailed review of the existing data on nanocages may be found in [22]). In our opinion, the gold nanorods are more promising for PPTT, particularly, because of the simplicity of their synthesis [12], if properly functionalised to reduce the toxicity of the initial particle stabiliser, cetyltrimethylammonium bromide (CTAB) [23]. The efficacy of gold nanorods as thermal-sensitizing agents was demonstrated in model experiments and calculations [24, 25] and in the *in vivo* experiments with inoculated tumours in mice [26].

To date the methods of conjugation of nanoparticles (including CTAB-coated gold nanorods) with various biomolecules are developed. The main problems are inhibiting of interaction of nanoparticles with cells of immune system, prolongation of their circulation in blood [27] aimed at enhancing the efficiency of the mechanism of passive accumulation (enhanced permeability and retention – EPaR [28]), and providing addressed (or vector) [29] delivery of the conjugates to biotargets. In particular, there are many papers on PPTT of cancer cells in the *in vivo* experiments with gold nanorods, functionalised with epidermal growth factor receptor antibodies [30], phosphatidylcholine [31], folic acid [32], etc. However, a number of unresolved problems still exist in the field of application of gold nanorods for PPTT in the *in vivo* experiments and, all the more so, in clinical oncology.

First, as mentioned in a number of papers [33, 34], the efficiency of PPTT in oncology in determined by a combination of factors: (i) selective accumulation of particles in the tumour due to the passive EPaR mechanism and optimal surface functionalisation; (ii) selective heating due to localisation in microvolumes and spectral selectivity of light-to-heat conversion due to plasmon resonance tuning; (iii) optimisation of the PPTT protocols with respect to the dose and the method of particle injection, the means of their accumulation and localisation control, the parameters and regimes of irradiation, as well as the monitoring of thermolysis characteristics. The problems related to the delivery of the optical radiation to the biotargets still remain urgent, too.

In contrast to a variety of publications, devoted to *in vitro* experiments, the number of publications on PPTT of tumours *in vivo* using gold nanorods is not large. In most papers the intravenous injection was used, and the enhancement of accumulation of particles in the tumour was achieved by funtionalisation of particles using the molecules of thiolated polyethylene glycol (PEG-thiol) [26, 34–38]. The active addressed delivery is still a rare exclusion [39]. To enhance the accumulation they also used microcapsulation of nanoparticles [40] or their direct injection into the tumour [41]; however, the latter technique is implementable only for tumours with available localisation.

Optimisation of photothermotherapy using phantoms and animal models [16, 42–44] is also a challenge. It is known that the essential destruction of a tumour tissue takes place only if its temperature exceeds 50 °C [2]. Therefore, from our point of view, choosing optimal doses of the injected particles and laser exposure is important to provide such heating of tumour tissues that leads exactly to photothermolysis of malignant cells rather than to general moderate hyperthermia.

The aim of the present paper is to study the photothermal effect and the spatio-temporal distribution of temperature in murine tissues with inoculated tumour and in model suspensions, depending on the dose of injected nanoparticles, their biodistribution and parameters of laser radiation.

2. Materials and methods

2.1. Synthesis and characterisation of PEG-coated gold nanorods

The following reagents were used in the work: silver nitrate $AgNO_3$ (higher than 99.9%, Aldrich, USA, 20.913-9), CTAB (96%, Fluka, USA, No. 52370), hydrogen tetrachloroauric acid $HAuCl_4$ (higher than 99%, Aldrich, USA), isoascorbic acid (higher than 99%, Fluka, USA), sodium borohydride (Sigma-Aldrich, USA), hydrochloric acid (extra-high purity, Vekton, Russia), potash (extra-high purity, Reachim, Russia), PEG-thiol (M_w = 5000, Nektar, USA), water (Milli Q).

At the first stage of the synthesis the successive mixing of 1 mL of CTAB (0.1 M), 25 μL $HAuCl_4$ (10 mM) and 100 μL of sodium borohydride (10 mM) was carried out. After adding $HAuCl_4$ the mixture changes colour from colourless to yellow, and after adding sodium borohydride the colour immediately changes to pale brown, which indicates the appearance of gold nanoparticles having the size 1–3 nm. The seminal solution was left without mixing, with the lid open, for 30–120 min. Then to 100 mL of CTAB solution (0.1 M) we successively added 2 mL of $HAuCl_4$ solution (10 mM), 1 mL of ascorbic acid solution (100 mM), 1 mL of hydrochloric acid (1M), and 1 mL of gold seeds. The resulting suspension was kept at the temperature 28 °C during 24 hours. As a result we obtained a suspension of CTAB-coated gold nanorods with gold concentration ~80 μg mL^{-1} and optical density 3.5–4 at the wavelength of plasmon resonance in the cuvette 1 cm long.

The obtained suspension of gold nanorods was centrifuged during 1 hour at 14000*g*. The sediment containing nanoparticles was dissolved in the same volume of water. To 100 mL of nanoparticles suspension 1 mL of potash solution (0.2 M) and 1 mL of PEG-thiol (1 mM) were added. The suspension was kept during 12 hours at the temperature 28 °C and centrifuged with the acceleration of 14000*g* during 1 hour. The sediment was dissolved in 100 mL of water. The centrifuging-dissolving cycle was repeated 5 times, after which the solution was concentrated to provide the required optical density at the plasmon resonance wavelength.

The geometrical parameters of nanorods were determined using the transmission electron microscopy image, obtained by means of the electron microscope Libra-120 (Carl Zeiss, Germany) (Fig. 1a). From Fig. 1a it is seen that, on average, the particles possess the shape of a cylinder with hemispherical ends. The shape variations, consisting in the reduced curvature of ends and the smaller diameter in the middle of the particle ('end-cap' and 'dog-bone' morphology [45]) for this sample are very small. For an ensemble of nearly 500 particles we determined the length L_i, the diameter d_i, and the aspect ratio $r_i = L_i/d_i$ for each particle. The mean values of the length (L) and the diameter (d) of the rods are 41 ± 8 nm and 10.2 ± 2 nm, respectively. In the inset in Fig. 1a, the histogram of the particle number distribution $\Delta N_i/\Delta r_i$ with respect to the aspect

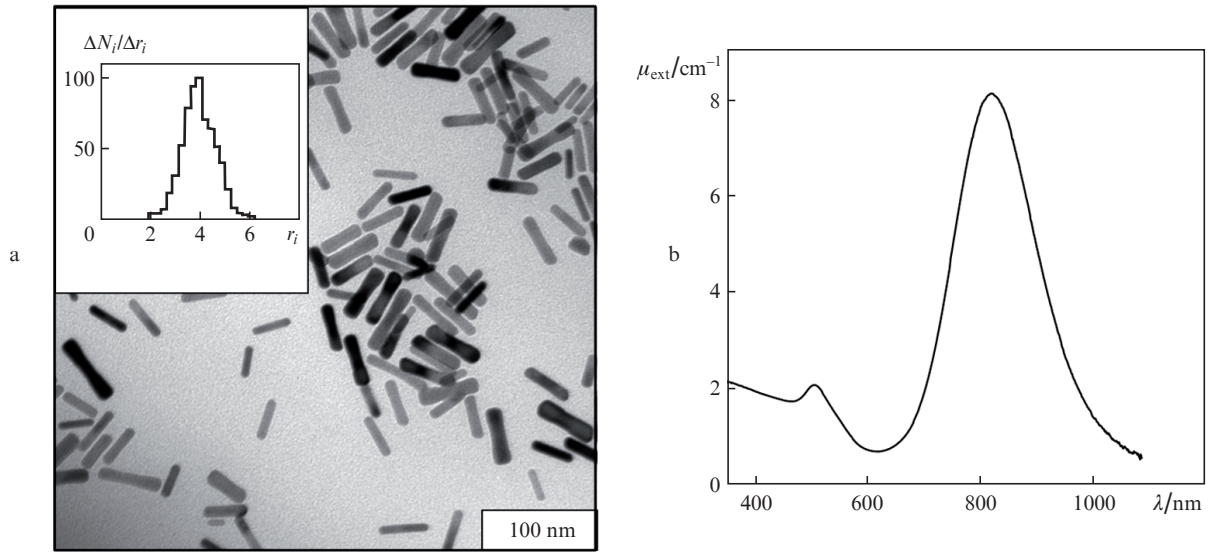

Figure 1. Transmission electron microscopic image (a) and extinction spectrum (b) of gold nanorods with the extinction index 8.16 cm^{-1} at the plasmon resonance wavelength 820 nm. In the inset the histogram of particle number distribution $\Delta N_i/\Delta r_i$ with respect to aspect ratios r_i with the mean value $r = 4.03 \pm 0.7$ is shown.

ratio r_i with the mean value $r = 4.03 \pm 0.7$ is presented. The optical properties of nanorods were verified using the extinction spectra measured with the UV-vis Specord 250 spectrophotometer (Analytik, Jena, Germany) (Fig. 1b). From the measured values of the sample extinction A_{ext} with the layer thickness l we determined the extinction index (in cm^{-1}) $\mu_{ext} = \ln 10(A_{ext}/l)$. From the data of Fig. 1b the wavelength of longitudinal plasmon resonance is 820 nm and the extinction index in resonance is 8.16 cm^{-1}.

The extinction indices of concentrated solutions of nanorods in the *in vivo* experiments at the plasmon resonance wavelength were equal nearly to 46 and 11.5 cm^{-1} (the optical densities in the cuvette 1 cm long being 20 and 5, respectively). The gold content in the samples of biotissue was determined using the method of atomic absorption spectroscopy (AAS) with the Dual Atomizer Zeeman AA iCE 3500 spectrophotometer (Thermo Scientific Inc., USA). To calibrate the spectrophotometer we used the solution of $HAuCl_4$ in HCl (0.1 M) or the solution of colloid gold with the known concentration of gold. In the second case the particles were dissolved in aqua regis ($HCl:HNO_3 = 3:1$). Both calibration procedures yielded similar results. The concentrations of gold in concentrated suspensions of PEG-coated gold nanorods with the extinction indices 46 and 11.5 cm^{-1} were equal nearly to 400 and 100 μg mL^{-1}, respectively.

2.2. Scheme of *in vivo* experiments

In the experiments we used female linear mice Balb/c received from the 'Stolbovaya' Nursery of the Russian Academy of Sciences (Moscow). At the beginning of the experiments their age was three months and the body mass was 20–22 g. Before and during the experiments the animals were kept in vivarium following the rules of the European Convention for the Protection of Vertebrate Animals used for Experimental and Other Scientific Purposes. To perform the studies the mice were divided into two experimental groups of 14 animals each, and two control groups of 6 animals each.

Ehrlich's ascites carcinoma was used as a model tumour, which was inoculated to all mice intramuscularly into the left hip. The volume of injected tumour suspension was equal to 0.2 mL with the total number of cells 2×10^6. On the 14th day after inoculation the mean volume of the tumour was 1.7 ± 0.3 cm^3.

In the *in vivo* experiments the animals of the first experimental group with mature tumour were subject to injection of 0.4 mL of suspension of gold nanorods with the gold concentration 100 μg mL^{-1} into the caudal vein. To the animals of the second experimental group a similar volume of suspension of nanorods with the concentration 400 μg mL^{-1} was injected. 0.4 mL of saline was injected into the caudal vein of the animals of the first and second control groups. With the volume of injected suspensions and the mean weight of animals taken into account, the content of gold in the injected dozes of nanoparticles was 40 and 160 μg and the mean specific dozes of injected gold per the animal weight unit was 2 and 8 mg kg^{-1}, respectively.

In 24 hours after the intravenous injection of gold nanoparticles the experiments on laser heating of tumour and symmetrical area of healthy tissue were performed. Before the experiments the tumour surface and the areas to be irradiated were epilated. The semiconductor laser LIMO (Dortmund, Germany) with the wavelength 810 nm and output power up to 30 W was used as a source of radiation. The animals from both experimental groups and one control group were exposed to laser radiation. The second control group of mice was not subject to any action. The irradiation was performed during 5 min with the 1.2-W output from the face of the optical fibre, the distance from the optical fibre face to the object was 27 mm, and the laser light spot area was 0.3 cm^2.

In an hour after the tumour heating a half of the animals from each experimental group was subject to euthanasia followed by sampling the tumour, muscle tissue, spleen and liver. The second half of the animals from experimental groups was left for observing the tumour development dynamics and survival estimation. From each control group

four mice were left for survival control and two mice were subject to euthanasia with sampling of muscle tissue, spleen and liver. In the sampled organs the accumulation of nanorods was determined by AAC measurement of gold content.

2.3. Measurement of temperature spatial distribution in the experiments with suspensions of nanorods *in vitro*

The initial suspensions of nanorods were placed into Eppendorf test tubes and irradiated with the semiconductor laser light at the wavelength 810 nm. The experiments were carried out with different concentrations of nanorods, the volume of the sample was 1.5 mL, the power density of the cw laser radiation was 1.2 W cm^{-2}. The test tube was fixed vertical and the laser radiation was incident vertically from above via an optical fibre (Fig. 2a). The separation between the fibre face and the surface of the liquid in the test tube was 3 cm. The irradiation was performed during 5 min with recording temperature each 10 s.

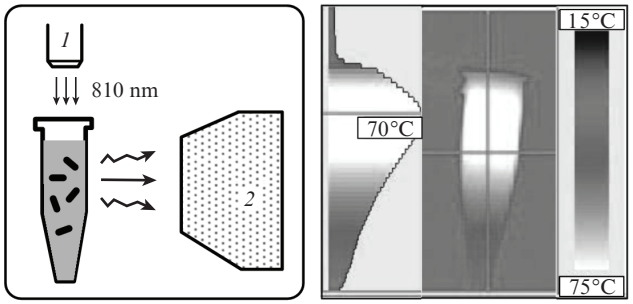

Figure 2. Scheme of experiments with nanorod suspensions, placed into Eppendorf test tube (a) and thermogram of temperature spatial distribution in this tube (b): (*1*) semiconductor laser; (*2*) IRSYS 4010 thermal imager.

When irradiating the test tubes with suspensions of nanorods, the temperature was noninvasively monitored using the IRISYS 4010 thermal imager (InfraRed Integrated system Ltd, Great Britain), placed at the distance 37 cm from the test tube. The spatial temperature distribution was recoded with the thermal imager placed aside the test tube in the direction, perpendicular to the laser beam (Fig. 2b).

The irradiation of experimental and control animal groups was carried out following the procedure described in Section 2.2. Noninvasive monitoring of the surface temperature in the experimental and control areas of tumour and normal tissues was performed using a thermal imager, as described in [16, 25].

3. Results and discussion

3.1. Photothermal effects in suspensions of gold nanorods

Figure 3 presents the distributions of temperature along the axes of test tubes with suspensions of gold nanorods with concentrations 8 and 100 μg mL^{-1}. Five measurements with a one-minute interval between them were performed after switching the laser on (up to the fifth minute) and three measurements (up to the 8th minute) – after the laser shutdown.

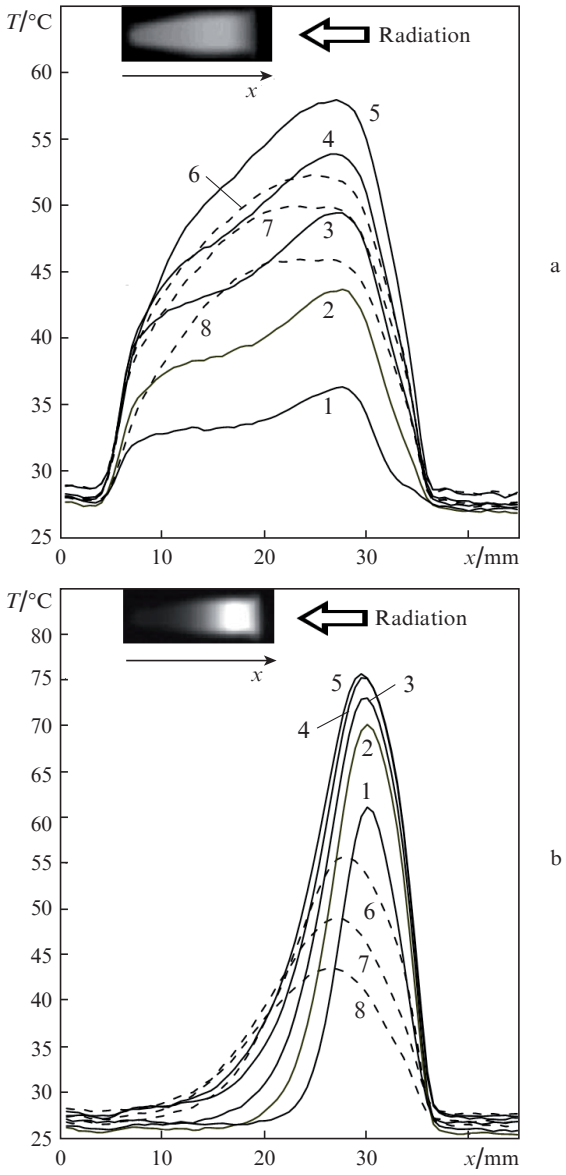

Figure 3. Distribution of temperature T along the axis x of test tubes under the laser heating of gold nanorod suspensions with concentrations 8 (a) and 100 μg mL^{-1} (b). The figures at the curves are the time values (in minutes) of the beginning of recording the temperature distribution after switching the laser on and off (laser action time is 5 min).

One can see from Fig. 3 that the maximal temperature for the concentration 8 μg mL^{-1} is 58 °C and for the concentration 100 μg mL^{-1} it is 76 °C. However, at high concentration of nanoparticles it appears impossible to heat the entire volume uniformly, because the laser radiation is absorbed when entering the sample and does not reach deeper layers of the suspension. In fact, the upper layer of high-concentration suspension is a screen in which practically all the heat absorbed by the nanoparticles is released. The heat transfer from upper layers to the lower ones occurs rather slowly; therefore, the heating of concentrated suspensions during the first five minutes is very nonuniform. On the other hand, for strongly diluted suspensions the heat release was more uniform over the volume, but very weak because of small number of nanoparticles. Therefore, an optimal concentration range exists within which the entire irradiated volume is heated with sufficient uniformity and efficiency. In the present experiment

the relative temperature increments differ only by 20%, while the concentration of nanoparticles varies by more than 10 times. The obtained results are important for understanding possible mechanisms of heat release under the conditions of the *in vivo* experiment. For example, it is clear that both small and large concentrations of particles in the biotargets are not optimal for photothermolysis.

3.2. Biodistribution of gold nanorods

Figure 4 presents diagrams of biodistribution of gold nanorods for two dozes of injected gold per animal weight unit (2 and 8 mg kg^{-1}), which correspond to the most probable range of dozes, used in the experiments on biotoxicity of gold nanoparticles [23]. However, it should be kept in mind that, according to the literature data [23], the absence of toxicity may be expected at short-time (about a week) course of injecting the particles with the daily dose of ~0.5 mg kg^{-1}. Hence, the doses used by us are somewhat higher than this toxicity limit. On the other hand, the successful PPTT experiment in mice with inoculated tumours [26] involved the doses of nanorods which were essentially higher (20 mg kg^{-1}).

From the presented data it is seen that the ratio of gold contents in all investigated tissues after injecting of suspensions of nanorods nearly corresponds to the ratio of the injected gold doses 1 4. In agreement with the existing literature data [23], the concentration of gold particles in the spleen and liver is almost by an order of magnitude higher than in the tumour and amounts to ~10% of the gold concentration in the injected suspensions. As in a similar in vivo model [37], our data show that the accumulation of gold nanorods in the spleen is much greater than in the liver. We would like to emphasise that as a result of selective accumulation the content of nanorods in liver (~35 μg g^{-1}) and spleen (~55 μg g^{-1}) is essentially higher than the mean injected dose (8 μg g^{-1}). Approximately the same ratio is observed for a smaller injected dose (2 μg g^{-1}). With the typical mean weight of the liver (~1.1 g) and spleen (~100 mg) in mice of the line Balb/c [46] taken into account, the total amount of gold in these organs is ~40 μg or 25% of the total injected dose 160 μg. This result is in reasonable agreement with the data obtained by T. Niidome team [37] for gold nanorods and with other literature data on biodistribution of gold nanoparticles [23]. Enhanced accumulation of gold nanorods in the liver and spleen is caused by the structure of these organs and physiological peculiarities of the vascular system. In liver the capillary vessels of fenestrated type prevail, while in the spleen the lacunae are present. Although the accumulation of gold in the spleen (in μg g^{-1}) is somewhat higher than in the liver, generally, the absolute amount of gold in the liver is greater due to the greater mass of the organ. Note also, that in [37] the gold nanorods in considerable amounts (nearly 50% of the accumulated in the liver) were found also in the murine lungs.

The content of gold in the tumour tissue amounts to ~1% of its concentration in the injected suspensions and exceeds the mean values for the healthy muscle tissue by three-four times. In other words, the content of gold per the unit of tumour mass is nearly 1 and 4 μg kg^{-1} for the injected doses 2 and 8 mg kg^{-1}, respectively. Therefore, even for passive accumulation of nanoparticles without their special functionalisation with targeting biomolecules, a considerable accumulation of nearly 50% of the mean dose of the injected nanoparticles is provided. The obtained data integrally agree with the data of other papers on biodistribution of nanorods due to passive accumulation of particles [35, 37, 38, 47].

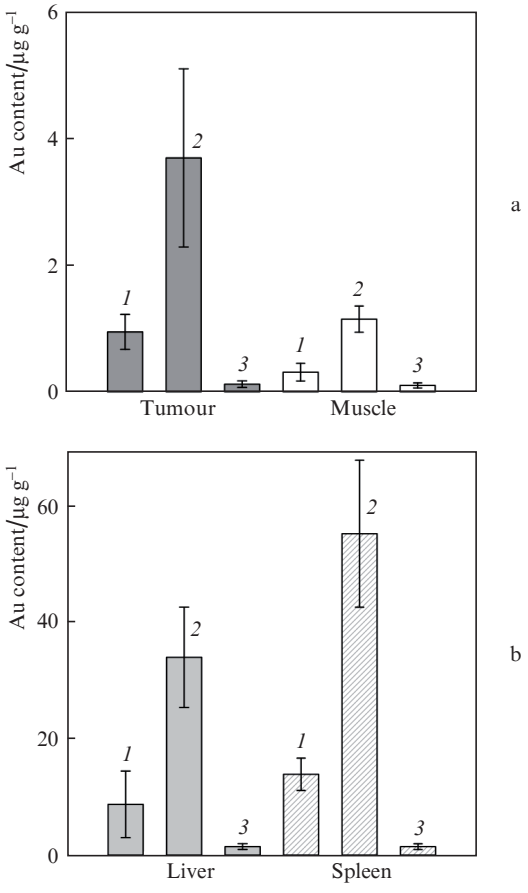

Figure 4. Biodistributions of gold nanorods in tumour and muscle (a), in liver and spleen (b) in 24 hours after intravenous injection of nanoparticles in doses 2 (*1*) and 8 mg kg^{-1} (*2*). Curve (*3*) shows the corresponding distribution when injecting saline instead of nanoparticles.

3.3. Photothermal effects in laser heating of gold nanorods *in vivo*

Figure 5 shows 2D distributions of temperature over the surface of murine skin at laser heating in 24 hours after systemic injection of gold nanorods. The thermal imager in these measurements remained in the same fixed position.

One can see from Fig. 5 that the distribution of temperature over the laser spot is nonuniform, which is determined by nonuniform distribution of the power density in the incident laser radiation and the processes of heat transfer from the hot regions to cold ones. The efficiency of laser heating is determined not only by the maximal temperature in the laser spot centre, but also by the diameter of the heated area, in which the temperature exceeds the given threshold value providing hyperthermia or thermolysis. In the present experiment the diameter of the region, in which the temperature exceeded 45 °C, was 7 mm in 1 min and 11 mm in 5 min after the beginning of irradiation. Figure 5d shows the temperature distributions along the horizontal axis (passing through the centre of the heated volume), obtained with the interval of 1 min after the beginning of irradiation and after the laser shutdown. The increase in the temperature distribution width is due to the processes of heat diffusion. After the laser shutdown the skin

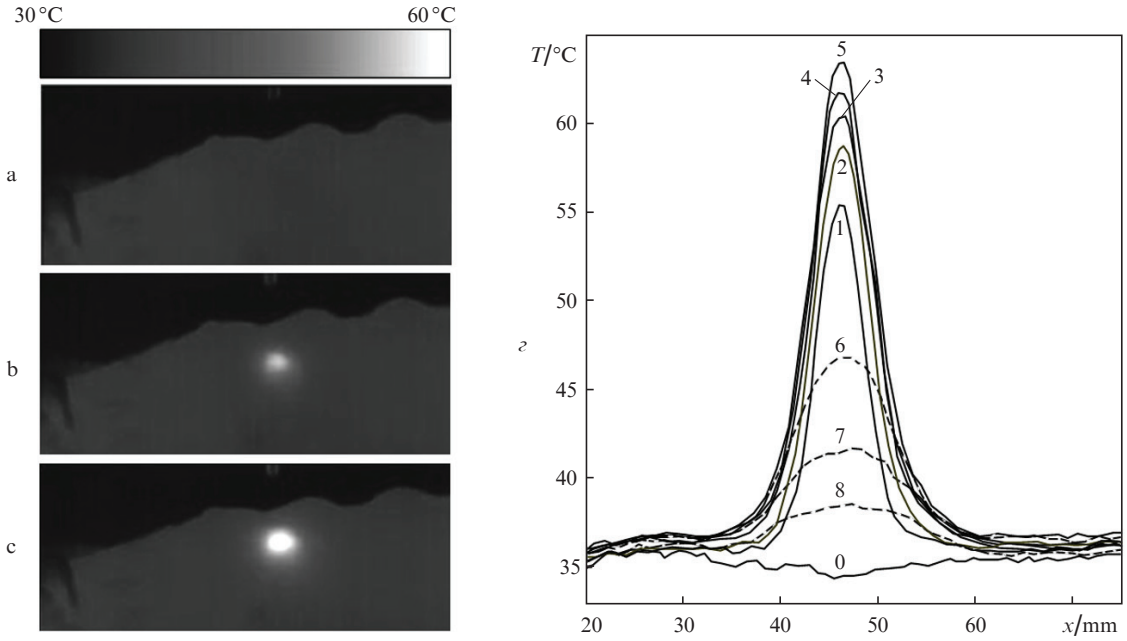

Figure 5. 2D distributions of temperature over the surface of murine skin before the laser irradiation (a), in 1 min (b), and 5 min (c) after the beginning of irradiation, obtained in 24 hours after systemic injection of gold nanoparticles in the dose of 8 μg g^{-1}. In Fig. 5d the distributions of temperature T along the horizontal axis (passing through the centre of the heated volume) are presented. The numbers at the curves show the time (in minutes) of starting the registration of temperature distribution before irradiation, after the beginning of irradiation and after the laser shutdown at the 5th min.

area cools slowly compared to the characteristic time of heating, and the temperature prolife becomes wider (smoother).

Figure 6 shows time dependences of the surface temperature of experimental and control skin regions, each curve being obtained by averaging the results from seven animals.

Even in the case of small dose of injected nanorods (2 mg kg^{-1}, Fig. 6a) we observed considerable difference in the temperature of the tumour tissue and the adjacent healthy area. After setting of the steady-state temperature this difference amounted to ~10 °C. For control the temperature of the skin surface was measured in the tumour zone and healthy tissue zone without injecting nanoparticles. No significant temperature difference between the healthy and tumour tissues was revealed without nanoparticles injected into them. Under the intravenous injection of nanorods in the small doze (2 mg kg^{-1}) the temperature of heated muscle tissue exceeded the control values by nearly 5 °C due to insignificant accumulation of particles in healthy muscle tissue, revealed in the experiments on biodistribution. The main increase of the temperature of the biotissue with nanoparticles introduced into it occurs during the first 100 s of laser heating, and then the rate of the temperature growth becomes significantly smaller.

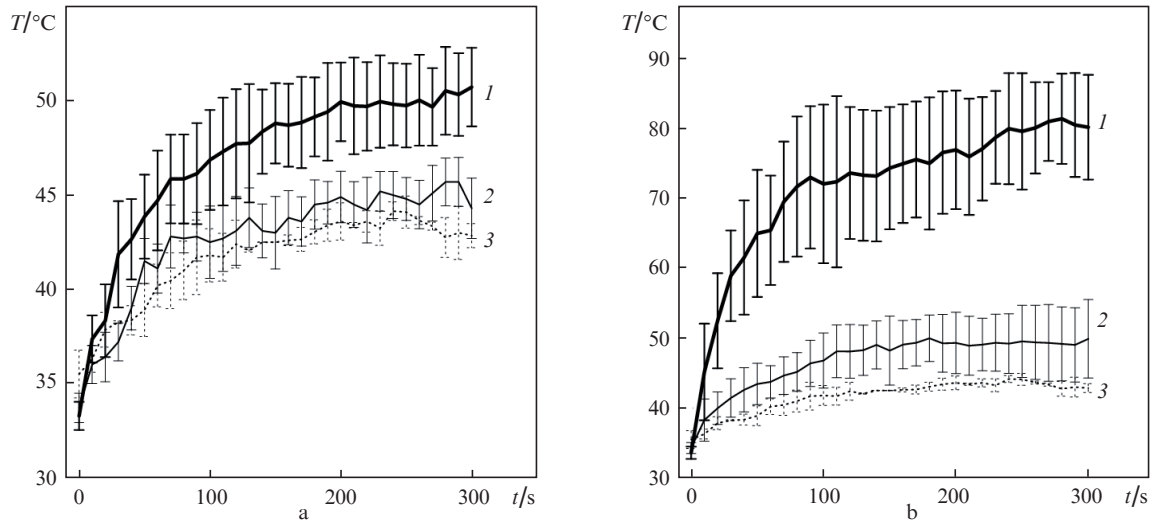

Figure 6. Kinetics of laser heating of tumour (*1*) and healthy (*2*) tissue in the vicinity of it maximum in 24 hours after intravenous injection of gold nanorods in the dose 2 (a) and 8 mg kg^{-1} (b). Curves (*3*) show the kinetics of the maximal heating of healthy muscle tissue without injecting the nanoparticles (control). The data are averaged over the experimental and control groups of animals.

One can see from Fig. 6b that due to the passive selective accumulation of nanorods in the case of their intravenous injection in the dose 8 mg kg^{-1} a strong increase in the tumour temperature occurs (by nearly 30 °C) as compared with the temperature of the adjacent area of a healthy tissue in the same animal. For this dose already after one–two minutes of laser irradiation the temperature of the tumour achieved ~70 °C, while for the dose of 2 mg kg^{-1} the maximal steady-state temperature was equal to ~50 °C.

Figure 7 presents the dependences of the temperature increment for suspensions and tumour tissue (*in vivo* experiment) on the concentration of gold nanoparticles. The temperature increment was measured after the fifth minute of irradiation, as described above. In the range of concentrations 0–10 μg mL^{-1} the temperature increment linearly depends on the concentration of gold nanoparticles in the suspension (Fig. 7, inset), and at larger concentrations the dependence becomes nonlinear and reaches a plateau. Taking into account that, practically, nanorods only absorb light rather than scatter it, the behaviour of curve (*1*) in Fig. 7 agrees with the Bouguer law $I_{abs}/I_0 = 1 - \exp(-\mu_{abs} l)$, where the absorption index of the suspension μ_{abs} is proportional to the concentration of particles.

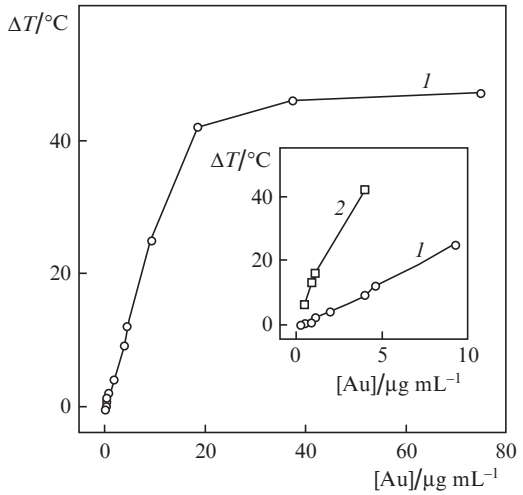

Figure 7. Dependences of the temperature increment ΔT on the concentration of gold nanorods in the suspension (*1*) and in the tumour tissue (*2*) after irradiation with laser light (810 nm, 1 W cm^{-2}) during 5 min.

Curve (*2*) in the inset, Fig. 7, corresponds to systemic injection of nanoparticles suspension, obtained by diluting the preparation with the concentration 40 μg mL^{-1}. The maximal concentration of gold in the tumour tissue was ~4 μg mL^{-1} i.e., fell within the range, corresponding to the linear growth of the temperature increment in the in vitro experiments. However, the observed temperature increments in the tissue with nanoparticles are by 5–25 °C higher than in the suspension having the same concentration of nanoparticles. The possible physical mechanisms, giving rise to this difference, are discussed in the next section.

3.4. Modelling of laser heating of a biotissue with introduced nanoparticles

According to the AAS data, the concentration of nanoparticles in the tumour does not exceed 1% (4 μg mL^{-1}) of the initial concentration of the injected particles 400 μg mL^{-1}. The extinction index of the suspension of nanorods with the concentration 4 μg mL^{-1} is equal to ~2 cm^{-1} at the wavelength of plasmon resonance. Experiments with heating aqueous suspensions of such concentrations have shown that the suspensions in test tubes are heated by 5–10 °C, i.e., since the volume fraction of the particles is so small, the heat, released from them, cannot essentially rise the temperature of the entire volume in the test tube. On the other hand, it follows from Figs 4, 6, and 7 that the tumour tissue with the mean content ~4 μg mL^{-1} of nanoparticles is heated very efficiently, the temperature increment being up to 80 °C during five minutes. Therefore, an apparent contradiction seems to exist between the data of heating experiments *in vivo* and *in vitro*.

The possible explanation of this disagreement is the following. First, the thermal imager registers IR radiation from the surface of an object and, correspondingly, displays the temperature distribution at the surface rather than in the bulk sample. For a biotissue the surface heating will be larger than for an aqueous suspension of nanoparticles, particularly, if their distribution is nonuniform, with stronger accumulation of particles within the surface layers of the tissue. Second, the thermal physical properties of biotissues, obviously, differ from those of water. In particular, many complex photothermal phenomena, accompanying the formation of bubbles of vapour in the aqueous medium under laser heating of plasmon nanoparticles [48], strongly depend on the parameters of the external medium. Third, in the tissues nanoparticles can form aggregates, in which the enhancement of photothermal effects is implemented via the electrodynamic interaction of nanoparticles at short distances [49].

Finally, an optical mechanism of the absorption enhancement, associated with multiple scattering, is possible. In contrast to water, the biotissue is a strongly (multiply) scattering medium. To calculate the optical properties of such media one can use both the analytic approaches, based on the radiative transfer equation, and the statistical modelling on the basis of the discrete photon concept, describing the multiple scattering and absorption of photons by means of the Monte Carlo method [50]. Within the framework of this approach the principal difference between a transparent and a strongly scattering medium is that in the second case the mean free path length of photons is essentially smaller than in the first case. Therefore, the rest conditions being the same, in the scattering medium the fraction of photons, absorbed in the course of multiple scattering, may be larger than in the transparent medium with the same amount of absorbing nanoparticles. In this case the important role is also played by the absorption of the diffusely scattered light by nanoparticles beyond the volume, irradiated by the incident beam. In the transparent medium the heat is produced practically only as a result of single absorption of radiation by nanoparticles within the beam volume. In correspondence with the discrete Monte Carlo model only a part of ballistic photons of the incident beam is absorbed, while in a scattering medium the additional contribution to heat release is caused by the absorption of multiply scattered photons in the entire sample. As far as we know, the mechanism of absorption enhancement due to multiple scattering, described above, was never discussed elsewhere in the context of PPTT problems, although the effects of multiple scattering in the system 'tissue+gold nanorods' were considered in connection with the problem of increasing the contrast in optical coherence tomography [51, 52].

The above qualitative explanation is illustrated by Fig. 8, which presents the results of Monte Carlo calculation of the fraction of absorbed photons in a scattering plane-parallel 1-cm-thick layer with chaotically oriented gold nanorods. The fraction of absorbed photons R_{abs} was calculated using the formula $R_{abs} = 1 - T - R$, where T is the transmission coefficient of the medium layer (taking both collimated and diffuse transmission into account), and R is the diffuse reflection coefficient. The number of traced photons was 10^5. The scattering properties of muscle biotissue [53] with its possible clearing [54] taken into account were simulated by an ensemble of light-scattering dielectric spheres in water. The diameter of the spheres was 600 nm, the refractive index 1.44, and their concentration was chosen to correspond to the range of extinction indices from 0 to 25 cm^{-1}. At the wavelength of 810 nm the extinction index of such a system practically coincides with the scattering index μ_{sc}.

The ensemble of gold nanorods was modelled by a set of chaotically oriented cylinders with hemispherical ends and Gaussian distribution of aspect ratios. As shown in [45], this model describes quite well the optical properties of the real sample of nanorods. The diameter of all cylinders is the same and equals 10 nm, the mean length is 40 nm, the mean aspect ratio is 4, and the width of the aspect ratio Gaussian distribution is 0.15. These parameters correspond to the nanoparticles with the plasmon resonance at the wavelength 810–820 nm, studied in the present paper. If the concentration of gold in the unit volume is 1 μg mL^{-1} (which corresponds to the concentration of nanorods $N = 1.8 \times 10^{10}$ cm^{-3}), then the ensemble of model nanoparticles has the following optical characteristics: the mean extinction index $\mu_{ext} = \mu_{abs} + \mu_{sc} = NC_{ext} = 0.0998$ cm^{-1} (C_{ext} being the integral cross-section of extinction); the mean absorption index $\mu_{abs} = NC_{abs} = 0.09805$ cm^{-1} (C_{abs} being the integral cross-section of absorption); the mean albedo $\overline{\omega} = \mu_{sc}/\mu_{ext} = 0.0175$; the mean scattering indicatrix practically coincides with the Rayleigh indicatrix $p(\theta) = (1 + \cos^2\theta)/2$. For other concentration of gold the indices of extinction and absorption are simply multiplied by this concentration (in μg mL^{-1}).

One can see from Fig. 8a that for a layer of nanorods in water with the concentration, corresponding to the extinction index 0.4 cm^{-1} (practically equal to the index of absorption) the fraction of absorbed photons amounts to 28.5%. If the same amount of nanoparticles is placed into a scattering biotissue, then the fraction of absorbed photons increases to ~39%, the scattering index being 5–15 cm^{-1}. For small scattering indices the results of calculations coincide with those, obtained for nanoparticles in water, while for large scattering indices the radiation is mainly backscattered diffusely and practically does not penetrate deep into the layer. This fact explains the existence of wide optimal range of extinction (scattering) index values for the biotissue (5–15 cm^{-1}) for which the fraction of absorbed photons approaches 40%, as well as the reduction of the absorbed photons fraction at large scattering indices of the biotissue ($\mu_{sc} > 60$ cm^{-1}).

Figure 8b presents the results of computer calculation of the fraction of absorbed photons R_{abs} depending on the concentration of gold nanoparticles in water and in the model biotissue. In correspondence with stated above, at small concentration of nanoparticles the value of R_{abs} is proportional to it (inset in Fig. 8b). In the model biotissue R_{abs} is higher than in water, if the concentration of particles is smaller than 20 μg mL^{-1}. At higher concentrations the opposite effect was observed, namely, in the suspension of nanoparticles the absorption is greater than in the model tissue with nanoparticles. This is due to the fact that at high concentrations of nanoparticles the radiation is absorbed and backscattered in the surface layers rather than penetrates into deep layers.

Thus, the computer modelling qualitatively confirms the contribution of multiple scattering into the enhancement of light absorption by nanoparticles. However, this contribution is limited by the range of biotissue scattering indices smaller than 60 cm^{-1}. Besides, the calculations carried out and the data of preliminary experiments show that the enhancement of absorption in a scattering medium does not explain strong difference in heating tissues and suspensions. An alternative explanation is that the concentration of gold nanoparticles in the peripheral regions of the tumour is higher than the bulk

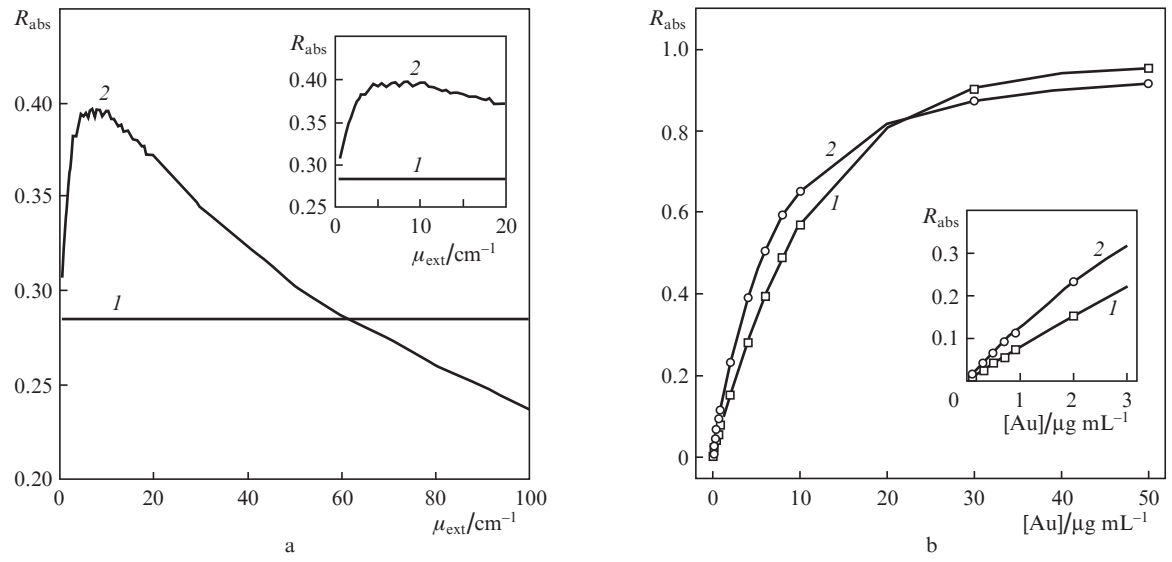

Figure 8. Dependences of the fraction of absorbed photons on the extinction index of the scattering biotissue, calculated using Monte Carlo method, for the concentration of gold nanorods 4 μg mL^{-1} (absorption index 0.4 cm^{-1}) (a) and on the concentration of gold nanorods for the scattering index of the biotissue 10 cm^{-1} (b) for aqueous suspension of nanorods (*1*) and for the biotissue with nanoparticles introduced into it (*2*).

value. An analogous effect was observed [55] in the histological studies of accumulating the gold-silver nanocages in a tumour. Therefore, the increase in the surface temperature, recorded by the thermal imager, may be caused by the increase in the released heat amount due to a higher peripheral concentration of particles. A more detailed analysis of the data of Fig. 7 requires additional studies, including modelling of thermal effects and variation of volume temperature distribution, which is beyond the scope of this paper.

3.5. The change in the tumour size in the process of PPTT

Figure 9 presents the dependences of the murine tumour volume on the time passed after the photothermotherapy. Laser irradiation of tumours under systemic injection of gold nanorods in the maximal dose of 8 μg g^{-1} resulted in an essential reduction of the tumour size in 9–12 days after PPTT. A strong rise of the temperature in this regime of PPTT caused thermal destruction (thermolysis) of the tumours. However, in the periphery of the tumours some undamaged regions were left, which became a source of further recession. In the case of a smaller dose (2 μg g^{-1}) the hyperthermia regime was implemented, and the deceleration of the tumour growth was minimal as compared with the control groups. The animals of the control group under laser action demonstrated even a stimulation of the tumour growth at the temperature ~40 °C, which agrees with the known literature data [1, 2].

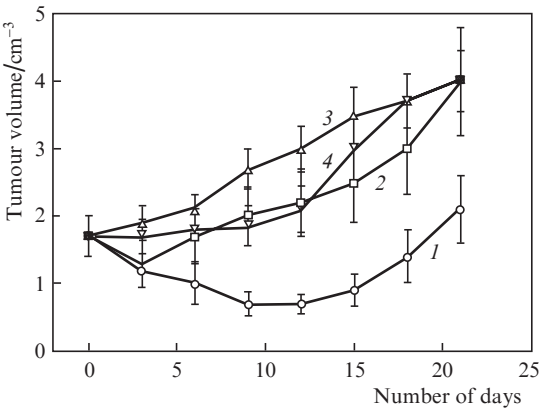

Figure 9. Dependences of the tumour mean volume on the number of days passed after performing the PPTT in the experimental groups with the dose of injected gold nanorods 8 (*1*) and 2 mg kg^{-1} (*2*), and for control groups with laser irradiation without injecting nanoparticles (*3*) and without laser irradiation (*4*).

4. Conclusions

The main results of the present paper are as follows:

(i) PEG-coated nanorods with the size 40 × 10 nm in 24 hours after systemic injection to mice with inoculated Ehrlich carcinoma are accumulated in the tumour in the amount of ~4 μg g^{-1} (1% of the concentration of the injected preparation). In 24 hours after the injection the concentration of nanoparticles is maximal in the spleen, somewhat smaller in the liver and exceeds the concentration of nanoparticles in the tumour nearly by 1–15 times. The content of gold in healthy muscle tissue is nearly 3–4 times smaller than in the tumour. In agreement with the published data [23, 26, 35, 47], our results confirm good contrast of accumulation of PEG-coated nanorods due to the passive accumulation mechanism (EPaR effect [28]) alone.

(ii) Too high concentrations of nanoparticles in the tumour may lead to undesirable effect of light absorption in surface layers and extremely nonuniform heat release. From the clinical point of view this limits the possibilities of using interstitial technique of introducing the gold nanoparticles into tumours at PPTT.

(iii) At the same mean concentrations of nanoparticles in suspensions and tumour tissues the laser heating of tissues (following the data of thermography) occurs with higher efficiency. This enhancement of laser heating in tissues with nanoparticles, introduced into them, may be related to a complex of causes, including the difference of thermal physical parameters of water and biotissue, aggregation of nanoparticles in tissues, and the influence of multiple scattering in the biotissue.

(iv) Accumulation of gold nanorods in the amount of 5–10 μg g^{-1} in the tumour tissue allows reduction of a power density of the laser radiation to 1–2 W cm^{-2}, which is nearly two times smaller than in the case of accumulation of nanoshells (4 W cm^{-2} [14]). Taking these data into account, one can suggest that the gold-silver nanocages may also be efficient thermal sensitisers for PPTT [55].

(v) In our opinion, weak hyperthermia using plasmon nanoparticles is low-efficient for tumour treatment. A more optimal approach is to provide thermodestruction (thermolysis) of the tumour by means of short-time fast heating of the tissues up to the tissue-destructing temperature. In our experiments, even in the case of significant photothermal action on the tumour tissue, its complete resorption was not achieved, and in 12 days after PPTT the growth of the tumour recommenced. These results again emphasise the necessity to use photothermotherapy in combination with chemotherapy and ray therapy in order to provide high efficiency of the complex therapy.

Acknowledgements. The authors are grateful to A.N. Bashkatov (N.G. Chernyshevsky Saratov State University) for discussion of optical properties of biotissues and their modelling by means of the Monte Carlo method. The work was partially supported by the Russian Foundation for Basic Research, the Programs of Presidium of Russian Academy of Sciences 'Fundamentals of Technology of Nanostructures and Nanomaterials' and 'Basic Research for Medicine', Federal Targeted Programme 'Scientific and Scientific-Pedagogical Personnel of Innovative Russia' (Contract Nos 14.740.11.260), by the grant of the RF President for State Support of Young Scientists (MK-1057.2011), and by the Government of the Russian Federation for State Support of Research conducted under the guidance of leading scientists in Russian educational institutions of higher professional education.

References

1. Habash R.W., Bansal R., Krewski D., Alhafid H.T. *Crit. Rev. Biomed. Eng*., **35**, 37 (2007).
2. Goldberg S.N., Gazelle G.S., Mueller P.R. *AJR Am. J. Roentgenol*., **174**, 323 (2000).
3. Huang X., Jain P.K., El-Sayed I.H., El-Sayed M.A. *Lasers Med. Sci*., **23**, 217 (2008).
4. Dreaden E.C., Mackey M.A., Huang X., Kang B., El-Sayed M.A. *Chem. Soc. Rev*., **40**, 3391 (2011).
5. Pitsillides C.M., Joe E.K., Wei X., Anderson R.R., Lin C.P. *Biophys. J*., **84**, 4023 (2003).

6. Hirsch L.R., Stafford R.J., Bankson J.A., Sershen S.R., Rivera B., Price R.E., Hazle J.D., Halas N.J., West J.L. *Proc. Natl. Acad. Sci. U.S.A.*, **100**, 13549 (2003).
7. Khlebtsov N.G. *Kvantovaya Elektron.*, **38**, 504 (2008) [*Quantum Electron.*, **38**, 504 (2008)].
8. Boisselier E., Astruc D. *Chem. Soc. Rev.*, **38**, 1759 (2009).
9. Khlebtsov N.G., Dykman L.A. *J. Quant. Spectrosc. Radiat. Transfer*., **111**, 1 (2010).
10. Hirsch L.R., Gobin A.M., Lowery A.R., Tam F., Drezek R.A., Halas N.J., West J.L. *Ann. Biomed. Eng*., **34**, 15 (2006).
11. Skrabalak S.E., Au L., Li X., Xia Y. *Nat. Protoc*., **2**, 2182 (2007).
12. Huang X., Neretina S., El-Sayed M.A. *Adv. Mater*., **21**, 4880 (2009).
13. Ratto F., Matteini P., Centi S., Rossi F., Pini R. *J. Biophotonics*, **4**, 64 (2011).
14. Lal S., Clare S.E., Halas N.J. *Acc. Chem. Res*., **41**, 1842 (2008).
15. Bardhan R., Lal S., Joshi A., Halas N. *Acc. Chem. Res*., **44**, 936 (2011).
16. Terentyuk G.S., Maslyakova G.N., Suleymanova L.V., Khlebtsov N.G., Khlebtsov B.N., Akchurin G.G., Maksimova I.L., Tuchin V.V. *J. Biomed. Opt*., **14**, 021016 (2009).
17. Schwartz J.A., Shetty A.M., Price R.E., Stafford R.J., Wang J.C., Uthamanthil R.K., Pham K., McNichols R.J., Coleman C.L., Payne J.D. *Cancer Res*., **69**, 1659 (2009).
18. Day E.S., Thompson P.A., Zhang L., Lewinski N.A., Ahmed N., Drezek R.A., Blaney S.M., West J.L. *J. Neurooncol*., **104**, 55 (2010).
19. http://clinicaltrials.gov/ct2/show/NCT00848042.
20. Chen J., Wang D., Xi J., Au L., Siekkinen A., Warsen A., Li Z.Y., Zhang H., Xia Y., Li X. *Nano Lett*., **7**, 1318 (2007).
21. Kim C., Cho E.C., Chen J., Song K.H., Au L., Favazza C., Zhang Q., Cobley C.M., Gao F., Xia Y., Wang L.V. *ACS Nano*, **4**, 4559 (2010).
22. Xia Y., Li W., Cobley C.M., Chen J., Xia X., Zhang Q., Yang M., Cho E.C., Brown P.K. *Acc. Chem. Re*s., **44**, 914 (2011).
23. Khlebtsov N.G., Dykman L.A. *Chem. Soc. Rev*., **40**, 1647 (2011).
24. Cole J.R., Mirin N.A., Knight M.W., Goofrich G.P., Halas N.J. *J. Phys. Chem. C*, **113**, 12090 (2009).
25. Khlebtsov B.N., Khanadeev V.A., Maksimova I.L., Terentyuk G.S., Khlebtsov N.G. *Rossiyskiye nanotekhnologii*, **5**, 54 (2010) [*Nanotechnologies in Russia*, **5**, 454 (2010)].
26. Von Maltzahn G., Park J.H., Agrawal A., Bandaru N.K., Das S.K., Bhatia S.N. *Cancer Res*., **69**, 3892 (2009).
27. Terentyuk G.S., Maslyakova G.N., Suleymanova L.V., Khlebtsov B.N., Kogan B.Ya., Akchurin G.G., Shantrocha A.V., Maksimova I.L., Khlebtsov N.G., Tuchin V.V. *J. Biophotonics*, **2**, 292 (2009).
28. Iyer A.K., Khaled G., Fang J., Maeda H. *Drug Discovery Today*, **11**, 812 (2006).
29. Llevot A., Astruc D. *Chem. Soc. Rev*., **41**, 242 (2012).
30. Huang X., El-Sayed I.H., El-Sayed M.A. *J. Am. Chem. Soc*., **128**, 2115 (2006).
31. Takahashi H., Niidome T., Nariai A., Niidome Y., Yamada S. *Chem. Lett*., **35**, 500 (2006).
32. Huff T.B., Tong L., Zhao Y., Hansen M.N., Cheng J.-X., Wei A. *Nanomedicine*, **2**, 125 (2007).
33. Kennedy L.C., Bickford L.R., Lewinski N.A., Coughlin A.J., Hu Y., Day E.S., West J.L., Drezek R.A. *Small*, **7**, 169 (2011).
34. Dykman L.A., Khlebtsov N.G. *Chem. Soc. Rev*., **41**, 2256 (2012).
35. Kogan B.Y., Andronova N.V., Khlebtsov N.G., Khlebtsov B.N., Rudoy V., Dement'eva O., Sedykh E., Bannykh L. *NSTI-Nanotech, Nanotechnology*, **2**, 65 (2008).
36. Sirotkina M.A., Elagin V.V., Shirmanova M.V., Bugrova M.L., Snopova L.B., Kamensky V.A., Nadtochenko V.A., Denisov N.N., Zagaynova E.V. *J. Biophotonics*, **3**, 718 (2010).
37. Akiyama Y., Mori T., Katayama Y., Niidome T. *J. Controlled Release*, **139**, 81 (2009).
38. Wang L., Li Y.F., Zhou L., Liu Y., Meng L., Zhang K., Wu X., Zhang L., Li B., Chen C. *Anal. Bioanal. Chem*., **396**, 1105 (2010).
39. Li Z., Huang P., Zhang X., Lin J., Yang S., Liu B., Gao F., Xi P., Ren Q., Cui D. *Mol. Pharmaceutics*, **7**, 94 (2010).
40. Kawano T., Niidome Y., Mori T., Katayama Y., Niidome T. *Bioconjugate Chem*., **20**, 209 (2009).
41. Dickerson E.B., Dreaden E.C., Huang X., El-Sayed I.H., Chu H., Pushpanketh S., McDonald J.F., El-Sayed M.A. *Cancer Lett*., **269**, 57 (2008).
42. Maksimova I.L., Akchurin G.G., Terentyuk G.S., Khlebtsov B.N., Akchurin G.G., Jr., Ermolaev I.A., Skaptsov A.A., Revzina E.M., Tuchin V.V., Khlebtsov N.G. *Kvantovaya Elektron*., **38**, 536 (2008) [*Quantum Electron*., **38**, 536 (2008)].
43. Richardson H.H., Carlson M.T., Tandler P.J., Hernandez P., Govorov A.O. *Nano Lett*., **9**, 1139 (2009).
44. Ratto F., Matteini P., Cini A., Centi S., Rossi F., Fusi F., Pini R. *J. Nanopart. Res*., **13**, 4337 (2011).
45. Khlebtsov B., Khanadeev V., Pylaev T., Khlebtsov N. *J. Phys. Chem. C*, **115**, 6317 (2011).
46. Freund Y.R., Riccio E.S., Phillips S.J., Dousman L., MacGregor J.T. *Toxicol. Sci*., **42**, 91 (1998).
47. Niidome T., Yamagata M., Okamoto Y., Akiyama Y., Takahishi H., Kawano T., Katayama Y., Niidome Y. *J. Controlled Release*, **114**, 343 (2006).
48. Lukianova-Hleb E., Hu Y., Latterini L., Tarpani L., Lee S., Drezek R.A., Hafner J.H., Lapotko D.O. *ACS Nano*, **4**, 2109 (2010).
49. Khlebtsov B.N., Zharov V.P., Melnikov A.G., Tuchin V.V., Khlebtsov N.G. *Nanotechnol*., **17**, 5167 (2006).
50. Wang L.-H., Jacques S.L., Zheng L.-Q. *Comput. Meth. Prog. Bio*., **47**, 131 (1995).
51. Oldenburg A.L., Hansen M.N., Zweifel D.A., Wei A., Boppart S.A. *Opt. Express*, **14**, 6724 (2006).
52. Troutman T.S., Barton J.K., Romanowski M. *Opt. Lett*., **32**, 1438 (2007).
53. Bashkatov A.N., Genina E.A., Tuchin V.V. *J. Innov. Opt. Health Sci.*, **4**, 9 (2011).
54. Tuchin V.V. *Tissue Optics: Light Scattering Methods and Instruments for Medical Diagnosis* (Bellingham, WA: SPIE Press, 2007, PM 166).
55. Chen J., Glaus C., Laforest R., Zhang Q., Yang M., Gidding M., Welch M.J., Xia Y. *Small*, **6**, 811 (2010).